NASA Technical Memorandum 103107
AIAA-90-1935

On the Use of External Burning to Reduce Aerospace Vehicle Transonic Drag

Charles J. Trefny
Lewis Research Center
Cleveland, Ohio

Prepared for the
26th Joint Propulsion Conference
cosponsored by the AIAA, ASME, SAE, and ASEE
Orlando, Florida, July 16-18, 1990

NASA

ON THE USE OF EXTERNAL BURNING TO REDUCE AEROSPACE VEHICLE TRANSONIC DRAG

Charles J. Trefny
NASA Lewis Research Center
Cleveland, Ohio 44135

Abstract

The external combustion of hydrogen to reduce the transonic drag of aerospace vehicles is currently being investigated. A preliminary analysis based on a constant-pressure control volume is discussed. Results indicate that the specific impulse of the external burning process rivals that of a turbojet and depends on the severity of the initial base drag as well as on the flight Mach number and the equivalence ratio. A test program was conducted to investigate hydrogen-air flame stability at the conditions of interest and to demonstrate drag reduction on a simple expansion ramp. Initial test results are presented and compared with the control-volume analysis. The expansion ramp surface pressure coefficient showed little variation with fuel pressure and altitude - in disagreement with the analysis. Flame stability results were encouraging and indicate that stable combustion is possible over an adequate range of conditions. Facility interference and chemical kinetics phenomena that make interpretation of subscale ground test data difficult are discussed.

Nomenclature

A	cross-sectional area normal to free stream
A_b	projected base area normal to free stream
A^*/A	function of Mach number
C_f	orifice flow coefficient
C_p	centerline pressure coefficient
D	characteristic diameter or length, ft
d^*	diameter of sonic fuel injection orifice
f/a	fuel-air ratio
I_{sp}	specific impulse, sec
L	length of expansion surface
M	Mach number
m_{H_2}	mass flow rate of hydrogen, lbm/sec
P	pressure, psia
P_{eb}	effective backpressure, psia
P/P_t	function of Mach number
Q	dynamic pressure, lb/ft^2 abs
R	gas constant
S	orifice spacing
T	temperature, °R
V	velocity, ft/sec
W	base width at station zero
X	distance downstream of fuel injection plane
Y	height of control volume
Y_b	projected base height
Y_p	jet penetration height
γ	ratio of specific heats
δ	flow deflection angle, rad
ϕ	equivalence ratio, $(f/a)/(f/a)_{stoichiometric}$

Subscripts:

b	base
c	control volume
f	fuel
t	total or stagnation
0	station zero (inflow control surface) or free stream
2	station two (outflow control surface)

Superscript:

*	sonic

Introduction

Interest in "transatmospheric" or "aerospace" vehicles has been revived in the United States after almost two decades of relative inactivity. Evolutionary advances in "scramjet" propulsion, materials, and computer modeling, along with current political support,[1] have set the stage for an aggressive program (the national aerospace plane, or NASP) to develop a revolutionary aircraft capable of flying into orbit after takeoff from a conventional runway. Ready access to space and very high-speed Earth transportation are but two of the obvious benefits of this technology. A single-stage-to-orbit (SSTO) concept is very attractive because of its operational simplicity and flexibility and its potential for reducing the cost of putting a payload into orbit.

The technical challenges facing the aerospace community are numerous, many of them related to the airbreathing propulsion system required to achieve orbit in a single stage. Liquid hydrogen fuel is widely accepted as the fuel of choice for hypersonic airbreathing propulsion because it has high heat capacity for engine and airframe cooling and a heat of combustion twice that of hydrocarbon fuels. One drawback of hydrogen is its low molecular weight, which results in a large cryogenic volume that must be highly integrated with the airframe and the propulsion system.

An artist's conception of the national aerospace plane, shown in Fig. 1, illustrates a typical highly integrated configuration with a large, scarfed, two-dimensional exhaust nozzle. The entire vehicle aft end acts as an expansion surface for the scarfed nozzle, providing a very high area ratio, which is exploited at the high nozzle pressure ratios associated with high Mach number and altitude. This large aft-facing area becomes a critical issue, however, at transonic and supersonic speeds,

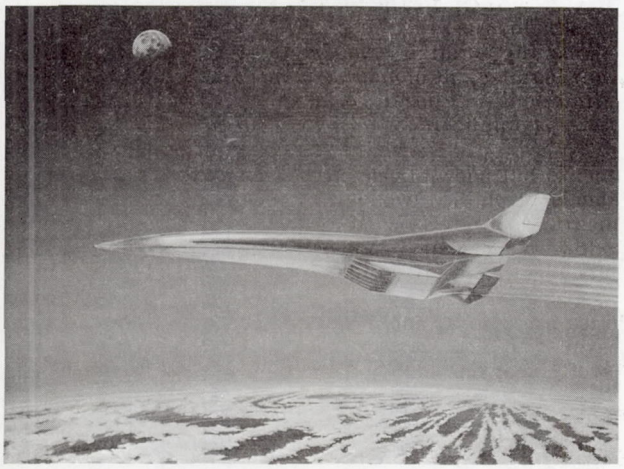

Fig. 1. Aerospace vehicle employing highly integrated exhaust nozzle.

where relatively low airbreathing-engine pressure ratios result in a highly overexpanded nozzle.

Designing a nozzle required to operate from takeoff to orbit is a formidable task. The amount of variable geometry that can be employed is a small fraction of that required to keep a nozzle "on design" over this speed range, mainly because of the invariability of the vehicle aft end, which must be used as the nozzle expansion surface. A discussion of nozzle design and operation, at least in qualitative terms, is necessary to understand the need for some type of augmentation at low-speed, off-design conditions. At hypersonic speeds, with the engine operating as a supersonic combustion ramjet or "scramjet," the combustor exit (nozzle inlet) Mach number is supersonic and one could envision a minimum-length, shock-free design with expansion to free-stream ambient pressure. Usually, however, the aircraft cannot accommodate the length and area ratio of such a design, and the expansion surface and the cowl are truncated. The resulting hypothetical design and associated flowfield are shown schematically in Fig. 2(a). The nozzle is underexpanded and the limiting characteristic in the exhaust flow emanating from the trailing edge of the cowl does not intersect with the expansion surface. As a result the free-stream Mach number has little effect on nozzle performance. In Fig. 2(b) the nozzle pressure ratio and the free-stream Mach number have been reduced to represent a transonic flight condition. The exhaust flow is highly overexpanded and the shear layer adjusts to an angle that equalizes pressure in the internal and external flows. The internal shock structure raises the pressure of the propulsive stream only to the local external pressure determined by the amount of turning in the external flow. Note that the cowl boattail always results in some initial turning and local pressure reduction (boattail drag).

To summarize, nozzle drag results when the exhaust flow overexpands upstream of the cowl trailing edge and is then unable to fully recompress because the free-stream flow turns around the aerodynamic shape formed by the cowl boattail and shear layer. This situation would, of course, be mitigated if some amount of variable geometry were available and the reduction in nozzle pressure ratio were not as severe. Also, the situation would be relieved somewhat by three-dimensional effects and local flow separations.

The nozzle pictured in Fig. 2 is a high-Mach-number, minimum-length design employing a sharp expansion at the nozzle throat, with a resulting geometric area ratio upstream of the cowl trailing edge. In the preceding discussion no attempt was made to vary the geometry over

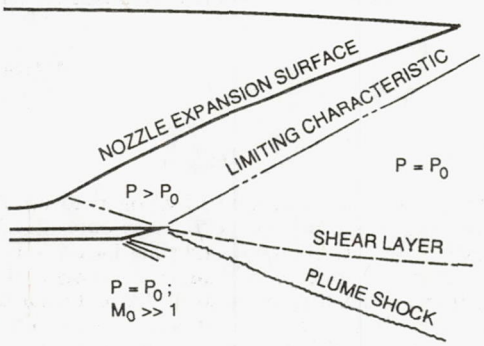

(a) Underexpanded at high flight Mach number.

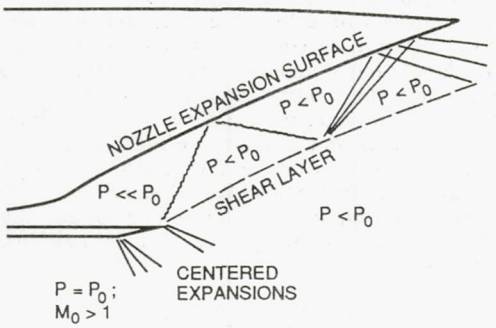

(b) Overexpanded at transonic flight Mach number.

Fig. 2. Qualitative nozzle flowfields.

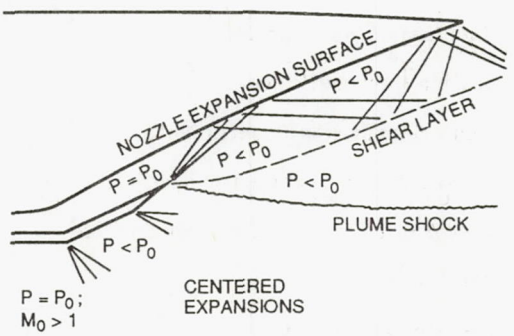

Fig. 3. Cowl flap deflection to prevent internal overexpansion.

the range of operating conditions, although one could envision deflecting the trailing edge of the cowl upward as shown in Fig. 3 to prevent internal overexpansion of the exhaust flow. Although drag occurring internally upstream of the cowl trailing edge may thus be reduced, the penalty paid for flap deflection is lower pressure and increased drag on the external flap surface. Note also that the pressure impressed on the exhaust flow at the cowl trailing edge is reduced, causing a more severe overexpansion in the external flow. A conceptually attractive solution shown in Fig. 4 would be the combustion of fuel in an external streamtube of air passing adjacent to the cowl. If the burning streamtube could be made to expand at free-stream pressure, the drag on the cowl flap would be eliminated and the exhaust flow would exit to ambient pressure without overexpanding.

This solution is highly conceptual at this point and depends on being able to realize a constant-pressure expansion of reacting fuel and air. The relative amounts of fuel and air required will be dictated by the geometric area ratio being compensated for as well as by free-stream conditions. The rate of heat release would also seem to be a critical variable and would depend on the

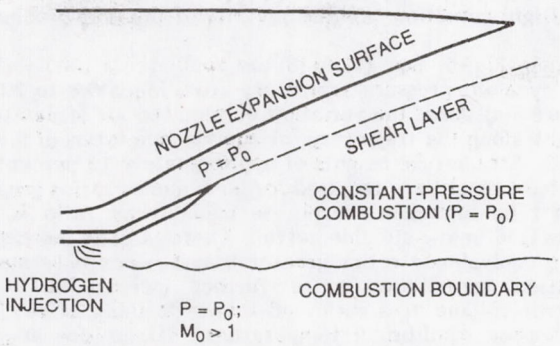

Fig. 4. Use of external burning with flap deflection to eliminate nozzle drag.

initial fuel distribution and subsequent rate of mixing between the fuel and the air. This, of course, assumes that the hydrogen-air chemical reactions proceed at a rate approaching equilibrium (i.e., the combustion process can be thought of as "mixing limited"). Related to this is the basic question of flame stability at the conditions of interest. Is there an altitude or Mach number limit for this process? If indeed a flameholder is required to initiate combustion at the low-pressure, low-temperature, high-velocity conditions existing outside the engine cowl, its drag must be a small fraction of the total drag reduction. Finally, assuming that the concept is workable, the potential performance in terms of fuel used per net drag force reduction should be estimated.

A review of the literature revealed that work related to this area falls roughly into two categories, "base burning," or combustion in the wake of projectiles to reduce drag, and "external burning," loosely defined by this author as the fueling and combustion of an airstream adjacent to an aerodynamic surface so as to actively control the pressure distribution on that surface. Most past work falls into the former category; Murthy, et al.[2] contains a bibliography with over 350 references. The present application tends more toward the external burning concept, which has been used to reduce drag, to provide control forces, and even to produce thrust.[3-11] Most of this work had been done, however, with pyrophoric fuels and free-stream Mach numbers higher than the present range of interest. The high heating value of hydrogen combined with constant-pressure (and therefore constant velocity) combustion in a transonic stream results in an interesting deviation from most past studies, since the Mach number in the burning stream may be reduced to a subsonic value solely by increasing the sonic velocity without the usual turning or shocks. The resulting highly complex flowfield is characterized by an embedded elliptic region that has little reason to "close" downstream of the aircraft because of the constant-velocity nature of the process. In the absence of velocity shear it seems that heat dissipation may be the only mechanism available to return the combustion products to a supersonic condition. Strahle[12] addressed this phenomenon analytically with a two-dimensional, small-perturbation analysis and concluded that a positive pressure coefficient could be maintained on a flat plate regardless of the transition to subsonic flow, but experimental verification was needed because the downstream boundary conditions could not be treated properly.

In order to make an initial assessment of the transonic drag reduction potential of external burning, a control-volume analysis was done to obtain a first-order estimate of performance and fuel flow requirements. An experimental program was then begun to resolve issues including flame stability and the validity of various assumptions used in the control-volume analysis. The balance of this paper presents and discusses the results of both the analysis and the experimental program.

Constant-Pressure, Control-Volume Analysis

A detailed analysis of external burning in a transonic flow would be a formidable task, characterized by mixing and finite-rate combustion of hydrogen and air, three-dimensional mixed supersonic-subsonic flowfields, and the interaction of at least three streams. External burning analysis methods of varying degrees of sophistication do appear in the literature,[13-20] but none are directly applicable to the current problem. In the present application of external burning, expanding combustion products must "fill" a void left by the vehicle base and the engine exhaust. To accomplish this, an amount of fuel must be burned with an appropriate amount of air - possibly at a specified rate. The size of the airstream that must be fueled and burned will be determined by the amount of expansion or the stream area ratio provided by the mass addition and combustion. It would seem that to completely relieve base drag, the free stream must be prevented from expanding into the base area. Therefore, the combustion products must occupy at least an area equal to the projected base area plus the cross-sectional area of the fueled airstream.

In order to quantify the amounts of fuel and air involved, as well as to assess the fuel injection problem, the control volume pictured in Fig. 5 was studied. The scenario just described corresponds to a flow deflection angle of zero and will be referred to as the "design" condition. The lower control surface is formed by the boundary between the fueled streamtube and the free stream. Strictly speaking, the upper control surface coincides with the main engine exhaust shear layer and any aft-facing cowl surface. The dynamics of the engine exhaust stream are neglected, however, so that the upper control surface is thought of simply as a solid body. Air at free-stream conditions flows through the inflow boundary, which is perpendicular to the free stream. Fuel is injected normal to the free stream downstream of the inflow plane, and combustion products flow out of the outflow plane, which is also perpendicular to the free stream. It is assumed that both inflow and outflow properties are uniform and that velocity is parallel to the free stream. At the design condition the entire control volume is assumed to be at the local static pressure in the free stream; thus, disturbances due to the injection of fuel, etc. are neglected.

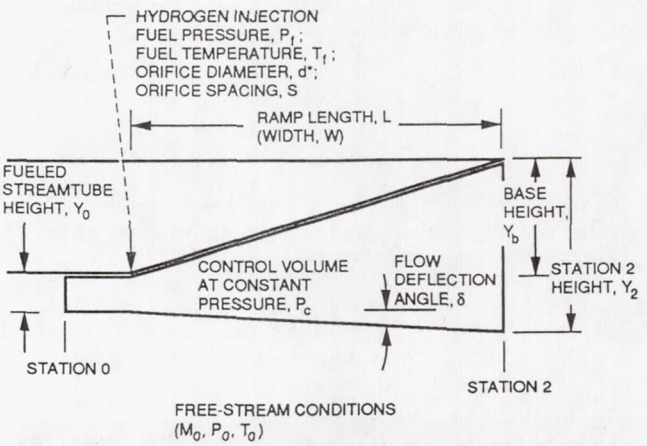

Fig. 5. Control-volume nomenclature.

The design condition of zero free-stream deflection angle results in the following geometric relation between the height of the streamtube of air that must be fueled and the area ratio obtained by combustion:

$$\frac{Y_0}{Y_b} = \frac{1}{\frac{Y_2}{Y_0} - 1} \tag{1}$$

Combining the continuity and momentum equations results in the following simple expression for the control-volume area ratio due to mass addition and combustion:

$$\frac{A_2}{A_0} = \frac{R_2}{R_0}\frac{T_2}{T_0}\left(1 + \frac{f}{a}\right)^2 \tag{2}$$

A noteworthy consequence of the constant-pressure assumption is that the ratio of inflow to outflow velocity given by the momentum equation is equal to 1 plus the fuel-air mass ratio. The stoichiometric fuel-air mass ratio for hydrogen and air is 0.02916, which results in an outflow velocity very nearly equal to the inflow or free-stream velocity. Because the ratio of inflow to outflow sound speed is about 3 for stoichiometric combustion, the outflow (or downstream) boundary condition for the transonic external burning process is nearly always subsonic. This has important implications in the interpretation of experimental results to be discussed later. The fuel-air ratio in Eq. (2) is considered an independent variable for the time being, and properties at the outflow boundary are assumed to be the equilibrium combustion products at this fuel-air ratio. The fuel flow required at the design condition is easily determined from the fuel-air (or equivalence) ratio and the size of the streamtube to be fueled (Eq. (1)). In terms of free-stream conditions the fuel flow per unit base area is given by

$$\frac{\dot{m}_{H_2}}{Y_b W} = 0.0155 \frac{P_{t,0}}{\sqrt{T_{t,0}}}\left(\frac{A^*}{A}\right)_0\left(\frac{Y_0}{Y_b}\right)\phi \tag{3}$$

Finally, the measure of goodness for external burning is taken as the net drag force reduction per unit fuel flow and is referred to herein as the specific impulse. The fuel flow comes directly from Eq. (3); the net drag force reduction requires further definition. At the design condition of zero drag the control-volume pressure is equal to the free-stream static pressure, and this pressure acts over an area equal to the aft-facing projected area of the body. By defining an "effective base pressure" P_b as the area-weighted average pressure acting on the aft-facing base surfaces without external burning, the specific impulse is defined as

$$I_{sp} = \frac{(P_0 - P_b)Y_b W}{\dot{m}_{H_2}} \tag{4}$$

In terms of the free-stream conditions, the equivalence ratio, and the control-volume area ratio given by Eq. (2), the specific impulse becomes

$$\frac{I_{sp}}{\left(1 - \frac{P_b}{P_0}\right)} = \frac{64.5}{\phi}\left(\frac{P}{P_t}\right)_0\left(\frac{A}{A^*}\right)_0\sqrt{T_{t,0}}\left(\frac{Y_2}{Y_0} - 1\right) \tag{5}$$

Examination of Eqs. (1) to (5) reveals that, under the assumptions discussed, the performance of the external burning concept depends on the equivalence ratio assumed, the flight condition, and the severity of the drag problem.

In Fig. 6, Eqs. (1) to (5) are applied to a 1000-lb/ft^2 abs dynamic pressure trajectory from Mach 0.8 to 2.6. Figure 6(a) shows the variation of required air streamtube height along the trajectory for equivalence ratios of 0.5, 1, and 2. Streamtube heights of approximately 10 percent of the base height are required for equivalence ratios greater than 1 but increase sharply as equivalence ratio is decreased below stoichiometric. There is little benefit in using equivalence ratios greater than 1, since only mass addition contributes to a further increase in control-volume area ratio and this is partially offset by decreasing equilibrium temperature. Streamtube height varies with free-stream Mach number because free-stream static temperature decreases as altitude increases; the colder the inflow, the larger the temperature ratio from combustion. Note that the curves become flat as the vehicle climbs into the tropopause at about Mach 1.75. The effect of different trajectories on the curves of Fig. 6(a) is slight and due only to the inflow temperature effect.

The required hydrogen flow per unit base area appears in Fig. 6(b). For equivalence ratios of 1 or less 0.1 to 0.2 lb/sec per square foot of base area is indicated. The required fuel flow increases more dramatically for rich mixtures as the streamtube height from Fig. 6(a) becomes almost constant. For trajectories other than the

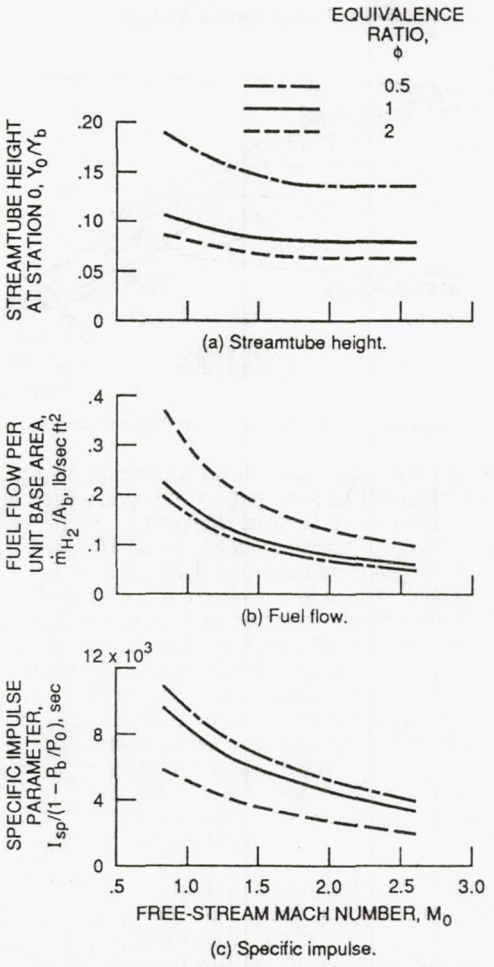

Fig. 6. Results for free-stream-pressure control volume. Dynamic pressure at station 0, Q_0, 1000 lb/ft^2 abs.

one shown the fuel flow is approximately proportional to the dynamic pressure, so that higher altitude trajectories would require less fuel.

A specific impulse parameter is plotted in Fig. 6(c) and is practically independent of trajectory. Low equivalence ratios give high performance but require that fuel be distributed over large streamtube cross-sectional areas. It appears, however, that performance does not suffer greatly with a stoichiometric system. Note that the absolute value of specific impulse depends on the severity of the drag problem; the lower the base pressure P_b, the higher the specific impulse. It should be remembered that these high performance numbers are based on drag reduction, with the potential for this high performance being generated by the main propulsion system.

Fuel Distribution Considerations

Given the required fuel flow and the height of the streamtube of air to be fueled, the mechanics of distributing the fuel can be examined. Normal injection from a row of sonic orifices is discussed here although many different variations, including the use of spraybars, are possible. It is assumed that the height of the streamtube to be fueled, given by Eq. (1), coincides with the jet penetration of the choked orifices. Many correlations describe the penetration of a highly underexpanded jet into a supersonic crossflow.[21-30] One that is particularly useful for this application is that of Povinelli, et al.[28] This correlation describes the contour representing a 5-percent volume concentration in the centerline plane of the injector and takes the following form for the case of normal, sonic injection and a thin approaching boundary layer:

$$\frac{Y_p}{d^*} = 1.12\left(\frac{P_f}{P_{eb}}\right)^{0.483}\left(\frac{X}{d^*} + 0.5\right)^{0.281} \qquad (6)$$

where the effective backpressure P_{eb} is taken to be two-thirds of the total pressure downstream of a normal shock at the free-stream Mach number for a supersonic free stream and two-thirds of the free-stream total pressure for a subsonic free stream. Equating the streamtube height with the height of the 5-percent hydrogen volume concentration at some distance downstream X/d^* of the injectors may at first seem tenuous, but it at least provides the proper variation of fueled streamtube height with changing free stream and fuel conditions. The value of X/d^* chosen will depend on details of the orifice and flameholder geometry and will allow the method to be calibrated. From experimental results on an expansion ramp, to be discussed in a subsequent section, an X/d^* of 30 seems to work reasonably well and is used henceforth.

The fuel flow rate for a choked injector can be written in terms of the fuel conditions and the orifice diameter:

$$\dot{m}_{H_2} = 0.1403\,\frac{P_f}{\sqrt{T_f}}\,\frac{\pi(d^*)^2}{4}\,C_f \qquad (7)$$

Equations (6) and (7) can now be combined to yield two parameters that are functions only of the desired equivalence ratio and the flight condition:

$$\left(\frac{d^*}{S}\right)\frac{P_f^{0.517}}{\sqrt{T_f}}\,C_f = \frac{10.16\left(\frac{\dot{m}_{H_2}}{Y_b W}\right)\left(\frac{X}{d^*} + 0.5\right)^{0.281}\left(\frac{Y_b}{Y_0}\right)}{P_{eb}^{0.483}} \qquad (8)$$

$$P_f^{0.483}\left(\frac{d^*}{Y_b}\right) = \frac{0.893\left(\frac{Y_0}{Y_b}\right)P_{eb}^{0.483}}{\left(\frac{X}{d^*} + 0.5\right)^{0.281}} \qquad (9)$$

As long as Eqs. (8) and (9) are satisfied, the streamtube height Y_0 from Fig. 6(a) will be injected with the appropriate amount of fuel from Fig. 6(b) consistent with the desired equivalence ratio. The actual distribution of fuel over the streamtube cross section will not be uniform, of course, and in this sense the equivalence ratio is of an average or "global" nature.

The performance shown in Fig. 6 was based on flight at constant dynamic pressure and streamtube equivalence ratio. With Eqs. (8) and (9) it is now possible to determine what schedule of fuel pressure and temperature is required to achieve a constant equivalence ratio over a range of Mach numbers, given an injector orifice diameter and spacing ratio (varying the orifice diameter and spacing ratio seems unlikely). Figure 7 shows such a schedule for a 1000-lb/ft^2 abs dynamic pressure flightpath and an equivalence ratio of 1. A significant variation in pressure and temperature is required for the particular injector geometry shown, which was chosen so as to keep the fuel temperature between about 500 and 1000 °R. Modulation of fuel pressure would be relatively easy as long as sufficient pressure were available in the fuel system, but the fuel temperature variation required probably will not match what is available in a power-balanced cycle. Some supplementary method of heating or cooling the hydrogen would have to be devised and would add weight and complexity to a system that must be carried to orbit after a short period of transonic operation. Obviously, other fuel schedules could be devised where the fuel conditions are relatively constant and the equivalence ratio varies, but as stated previously, equivalence ratios of approximately 1 are desirable. It is apparent that an "analysis" model of the external burning system is needed where fuel conditions and geometry are the independent

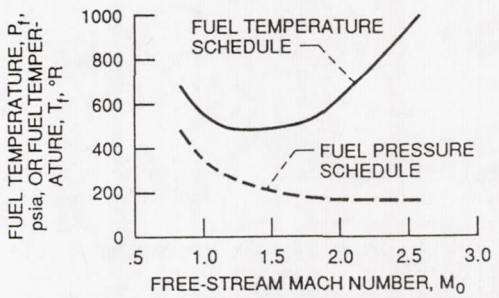

Fig. 7. Constant-equivalence-ratio (ϕ = 1) fuel injection schedule. Dynamic pressure at station 0, Q_0, 1000 lb/ft^2 abs; ratio of orifice spacing to orifice diameter, S/d*, 7.56; ratio of orifice diameter to projected base height, d^*/Y_b, 0.00694.

variables and the resulting equivalence ratio, control-volume pressure, and specific impulse are predicted. This involves some additional modeling.

Off-Design Performance Prediction

For the case where the inflow static pressure is different from the control-volume pressure and the free-stream deflection angle is nonzero (Eq. (1) no longer holds), combining the momentum and continuity equations yields the following equation for the control-volume area ratio:

$$\frac{A_2}{A_0} = \frac{\frac{R_2}{R_0}\frac{T_2}{T_0}\left(1 + \frac{f}{a}\right)^2}{\left(\frac{P_c}{P_0}\right)\left[1 + \frac{1}{\gamma_0 M_0^2}\left(1 - \frac{P_c}{P_0}\right)\right]} \qquad (10)$$

Note that this equation is identical to Eq. (2) except for the denominator, which involves the ratio of control-volume to free-stream pressure. Ultimately, this pressure ratio will be determined on the basis of the free-stream Mach number and a flow deflection angle. But first, the relationship between the control-volume area ratio given by Eq. (10) and the flow deflection angle must be determined. This is accomplished by assuming that the expansion is three dimensional, from the rectangle defined by the jet penetration height and the width of the expansion surface at station 0 to an appropriate rectangle at station 2, such that the area ratio defined by Eq. (10) is satisfied and the three sides of the control volume in contact with the free stream are at equal angles with the free stream. Since the control surfaces are all considered to be planar, this results in a streamtube area distribution that is quadratic in the axial direction and implies a quadratic temperature distribution as well. Whether or not this is physically realistic is beyond the scope of this simple analysis, but at least the three-dimensional "relieving" effect is accounted for approximately.

Now, the pressure throughout the control volume is considered to be equal to the pressure in the free stream after a turn through the deflection angle, as discussed previously. For supersonic flow small deflection angles are assumed and the pressure-versus-deflection-angle relation from linear theory is used:

$$\frac{P_c}{P_0} = 1 + \frac{\gamma_0 M_0^2 \delta}{\left(M_0^2 - 1\right)^{1/2}} \qquad (11)$$

For subsonic flow the problem is not quite as clearcut, but an approximation can be obtained by assuming incompressible flow over a wedge for which the velocity potential and stream function are known. Briefly, the pressure distribution corrected for compressibility is used to obtain the area-weighted average pressure acting on the deflected control surfaces. The final result is an expression for the control-volume pressure in terms of the free-stream Mach number and the deflection angle:

$$\frac{P_c}{P_0} = 1 + \frac{M_0^2}{\left(1 - M_0^2\right)^{1/2}}\left(\frac{\delta}{\delta + \pi}\right) \qquad (12)$$

The off-design or general problem of predicting the control-volume pressure given fuel conditions, orifice geometry, expansion surface geometry, and flight conditions can now be solved. First, the equivalence ratio is estimated by ratioing the fuel flow through one choked orifice to the amount of air at free-stream conditions passing through a rectangle of width equal to the orifice spacing and height equal to the jet penetration. Figure 8(a) shows the variation of equivalence ratio with Mach number on the 1000-lb/ft^2 abs trajectory for a constant fuel pressure and temperature that correspond to the Mach 1.4 design point of Fig. 7. Also shown for comparison is the constant equivalence ratio obtained by varying the fuel conditions as per the Fig. 7 schedule. The equivalence ratio increases continuously as the jet penetration (and airflow) decrease at constant fuel flow. The station 2 properties after equilibrium combustion can now be determined, and Eq. (10) is used to determine the deflection angle. Note that Eq. (10) contains the control-volume pressure ratio so that an iterative solution using Eq. (11) or (12) is required. In Fig. 8(b) the control-volume pressure ratio so obtained is plotted, along with the design pressure ratio of 1. Note that additional geometric parameters describing the expansion surface adjacent to the upper control surface must now be specified. For Mach numbers less than 1.4, negative deflection angles result and control-volume pressures are below ambient. For Mach numbers greater than 1.4, the control-volume area ratio is sufficient to cause a positive deflection angle in spite of decreasing jet penetration and

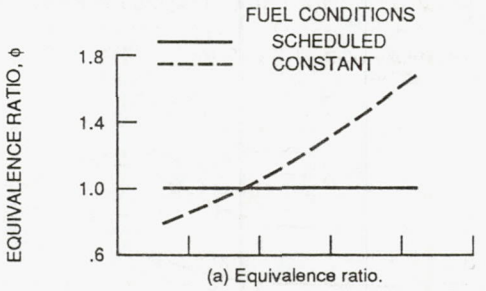

(a) Equivalence ratio.

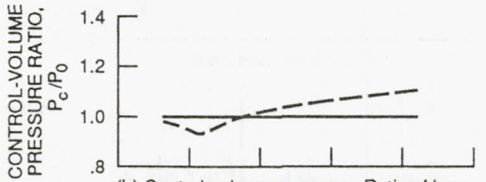

(b) Control-volume pressure. Ratio of base width at station 0 to projected base height, $W/Y_b = 2.5$; ratio of length of expansion surface to projected base height, $L/Y_b = 5$.

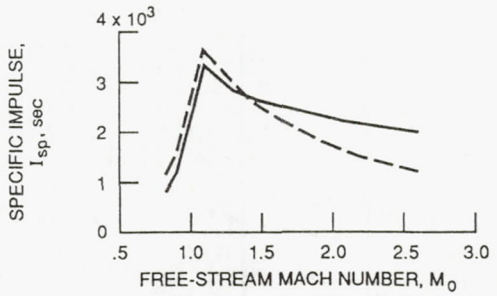

(c) Specific impulse; $W/Y_b = 2.5$; $L/Y_b = 5$.

Fig. 8. Performance of example geometry. Dynamic pressure at station 0, Q_0, 1000 lb/ft^2 abs; ratio of orifice spacing to orifice diameter, S/d*, 7.56; ratio of orifice diameter to projected base height, d^*/Y_b, 0.00694.

station 0 area. The definition of specific impulse must be modified slightly, since the control-volume pressure is not, in general, equal to the free-stream static pressure. In equation form the new definition is

$$I_{sp} = \frac{(P_c - P_b)Y_b W}{\dot{m}_{H_2}} \qquad (13)$$

The base pressure without burning P_b has been quantified by using the expansion ramp angle and Eq. (12) for subsonic flow and a Prandtl-Meyer expansion for supersonic flow. This allows the absolute value of specific impulse to be plotted for comparison with other forms of propulsion that may be under consideration. Figure 8(c) compares performance at constant fuel pressure and temperature with design performance. It is apparent that specific impulse is higher at points where the drag has not been completely eliminated (control-volume pressure is less than free-stream pressure) and lower where thrust is produced. Obviously, only two of the many possible fuel schedules have been explored here; the most advantageous operating conditions will have to be determined on the basis of many factors related to the overall cycle and mission. It does appear, however, that transonic drag reduction by the external combustion of hydrogen has the potential for very high performance within the assumptions of the preceding analysis. Specific impulse values rivaling those of a turbojet are indicated for a relatively simple, lightweight system. One might even be tempted to ask why external burning is not used as the primary propulsion system. The answer lies in the fact that external burning is a very efficient drag reduction device, exploiting the vacuum left by the vehicle base. This vacuum and the accompanying drag reduction potential are provided by the main propulsion system.

Experimental Program

Given the high performance potential indicated by the preceding simple analysis, an ongoing experimental program is being conducted. Two series of tests have been completed and results are presented here. In the first series simple hydrogen spraybars were tested in a Mach 1.26 stream to investigate the practicality of igniting and burning hydrogen at transonic, altitude conditions and also to begin to define the stability, or "flameout," limits of the process. An expansion ramp configuration was tested in the second series of tests; fuel was injected through normal, choked orifices to provide calibration and verification information for the analysis procedure.

Facility Description

The facility used for this investigation was the Propulsion Systems Laboratory cell 4 (PSL-4) at the NASA Lewis Research Center. PSL-4 is a continuous-flow, 25-ft-diameter altitude test chamber primarily used for direct-connect, full-scale turbine engine testing. It has been recently modified to provide the high pressures and temperatures representative of compressor face conditions at Mach 5 through use of a hydrogen-burning air preheater with oxygen makeup. Figure 9 shows the test cell with the modification installed. In the present investigation the hydrogen preheater was not used, since only transonic test conditions were needed. A 12-in.-exit-diameter, Mach 1.26 free-jet nozzle was bolted to the left end flange of the 48-in.-diameter flow-conditioning duct shown in the center of the photograph (the free-jet nozzle itself is not visible). The air normally used as combustion air for a turbine engine now flows through the free jet and becomes a transonic test medium. The free-jet air, any

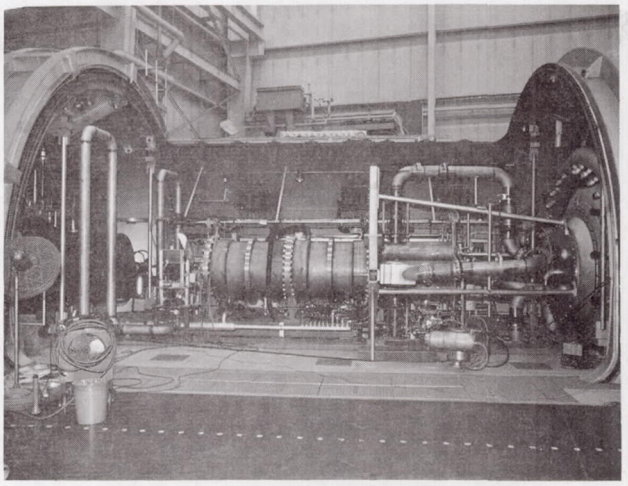

Fig. 9. Propulsion Systems Laboratory cell 4 (PSL-4).

combustion products, and test cell cooling and dilution air (required for safety) are all exhausted through a 55-in.-diameter exhaust collector duct located 63 in. downstream of the free-jet exit. The facility in this configuration is able to provide a Mach 1.26 stream at exit static pressures of 12 to 2 psia (5500 to 45 000 ft pressure altitude) and total temperatures from 540 to 1000 °R by using a heat exchanger system outside the test cell. This results in free-jet exit velocities of 1140 to 1550 ft/sec.

A schlieren system providing a 12-in.-wide by 6-in.-high field of view was set up at the free-jet exit. Despite efforts to isolate the schlieren support system from the test cell, it was only of marginal value owing to airflow-induced vibrations. An infrared video camera was also mounted at the free-jet exit to obtain images of the combustion process. The indium-antimonide detector, with a 2.0- to 5.6-μm range, provided good images of the 2.6-μm water vapor emission. A translating water-cooled total temperature probe located 18 in. downstream of the free-jet exit provided total temperature profiles from 8 in. below the free-jet centerline (completely out of the free-jet flow) to 2 in. above in a vertical centerline plane. The thermocouple, an iridium - 40 percent rhodium/ iridium "bare wire in crossflow" type, registered temperatures of over 4000 °R. These temperature measurements were used to approximately calibrate some of the infrared images in order to make temperature contour maps of the plume.

Hydrogen fuel was provided from high-pressure tube trailers located outside the building. The fuel circuit included a small gas generator to raise the temperature of the fuel to a maximum of 1500 °R by burning it with a small amount of air. Spark ignition was used to ignite both the spraybar and expansion ramp models. Various methods of attaching spark plugs and electrodes directly to the models were tried, but few survived the high temperatures. The method eventually made to work consistently was a translating spark ignitor system visible in Fig. 11. Essentially a spark plug attached to the end of a stainless steel tube, the electrodes were translated to a predetermined location by an air cylinder and then completely withdrawn from the free-jet flow after model ignition.

Spraybar Tests

Apparatus and procedure. - The objectives of the spraybar tests were to demonstrate that ignition and stable, external combustion of hydrogen in a transonic

flow is possible at altitude and to determine stability limits. The spraybars were designed to give equivalence ratios of 0.2 to 1.4. The equivalence ratio is based on the fuel flow through a choked orifice and an airflow at free-stream conditions that would pass through a rectangular area of height equal to the orifice jet penetration and of width equal to the orifice spacing. The jet penetration for this case was evaluated at an X/d* of 10. The equivalence ratio as defined here is a global value used primarily as a correlating parameter and not meant to accurately represent the nonuniform fuel distribution in the plane 10 diameters downstream of the injectors. The spraybar scale was made as large as possible given the size of the free jet and hydrogen safety considerations. Two spraybars 5/8 in. high were built, each with a cylindrical leading edge and a flat trailing edge. This cross section was maintained across the free-jet diameter, with fuel injection confined to the center 6 in. A total of six 0.1-in.-diameter main fuel injectors were used on both models, three facing up and three down, injecting fuel normal to the free stream. One of the models had fifteen 0.02-in.-diameter pilot orifices drilled into the flat trailing edge, injecting about 10 percent of the total fuel flow directly into the wake. This was the only difference between the two spraybars. Details of the spraybar configurations are presented in Fig. 10. Figure 11 shows the spraybar with pilots in position across the free jet. The translating ignitor and the water-cooled probe are also visible.

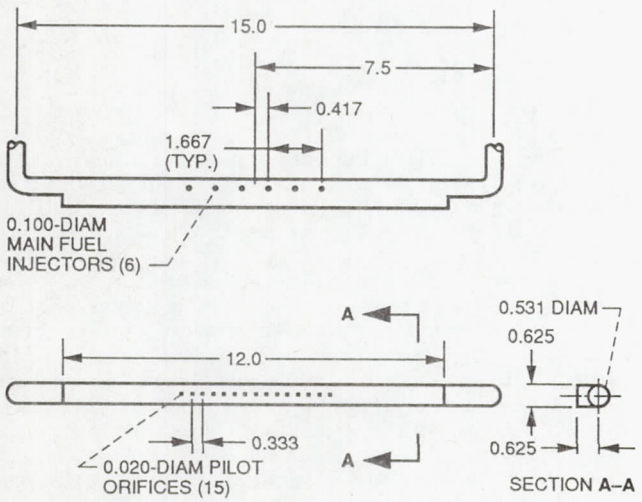

Fig. 10. Details of spraybar and fuel injector. (Dimensions are in inches.)

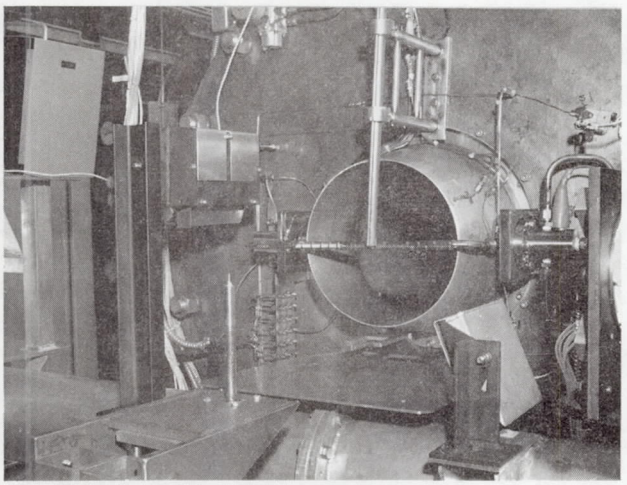

Fig. 11. Spraybar mounted in free jet.

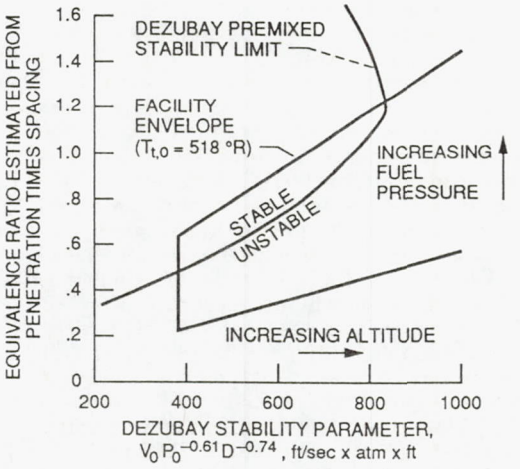

Fig. 12. Envelope of spraybar operating conditions.

An envelope of spraybar operating conditions based on available fuel pressures and facility conditions is shown in Fig. 12. A particular free-jet exit static pressure corresponds to a unique value of the DeZubay[31] stability parameter for a given free-jet total temperature. At a particular free-jet operating point, decreasing the fuel pressure decreases the equivalence ratio, since the fuel flow is proportional to the fuel pressure and the area on which the airflow is based depends on the jet penetration, which is proportional to approximately the square root of the fuel pressure (actually the 0.483 power - see Eq. (6)). The DeZubay stability limit curve is an experimentally determined correlation for a premixed hydrogen-air stream and a disk flameholder. The diameter in the DeZubay parameter is taken as the spraybar height (5/8 in.). As is the case with the equivalence ratio the DeZubay parameter is meant only as a correlator, and the stability limit curve is meant to show only an expected trend.

Initially, the test procedure was to set the desired free-jet operating point (matching the free-jet exit static pressure and the test cell pressure), ignite the model at maximum fuel pressure, and then reduce the fuel pressure until flameout occurred. Igniting the model at the Mach 1.26 free-jet design condition proved to be difficult and was only possible with the fuel preheated to 1500 °R by the gas generator. The procedure finally adopted was to set the test cell pressure at 12 psia and overexpand the free jet (reduce the supply pressure) until a Mach number of approximately 0.6 resulted at the exit. Both models ignited easily with ambient temperature fuel at this condition. After model ignition free-jet supply pressure was increased to the design value, and then both free-jet supply and test cell pressures were reduced simultaneously to the desired value of the DeZubay parameter, at which point the fuel pressure was reduced from maximum to flameout.

Results. - The points at which flameouts occurred for the piloted spraybar are shown in Fig. 13. The spraybar without pilots would not sustain combustion at the design free-jet Mach number, consistently extinguishing as the free-jet supply pressure was increased after ignition. Keeping the free jet on design while simultaneously reducing the test cell pressure and the free-jet supply pressure was difficult because two separate control valves and operators were used. Occasionally, a flameout at high fuel pressure would occur during this process when the free jet strayed off design. These points are depicted as solid symbols in Fig. 13. The

open symbols fall into a band that exhibits the same trend as the premixed stability curve, except for the point at elevated free-jet temperature, which was stable to a much lower fuel pressure. The stability parameter has no explicit temperature dependence, however; and the higher temperature simply results in a higher velocity and an apparently more severe condition with no allowance for changes in reaction rates.

Since the DeZubay parameter seems to be adequate for ambient temperatures, it was used to construct Fig. 14, where lines of constant DeZubay parameter are overlaid on an altitude-versus-Mach-number plot for a flameholder dimension of 1 in. In Fig. 13 a DeZubay parameter value of about 1000 could be construed as a practical limit for a slightly fuel-rich design. This limit is reached at Mach 1.5 for a 500-lb/ft^2 abs dynamic pressure trajectory, and at Mach 2.4 for 2000 lb/ft^2 abs. These limits, of course, increase with increases in flameholder dimension, but another practical limit of 2-psia static pressure is also shown beyond which stable combustion is unlikely regardless of the flameholder size. The preceding results indicate that ignition and flame stability must be carefully considered in the design of the external burning system but will not preclude its successful operation.

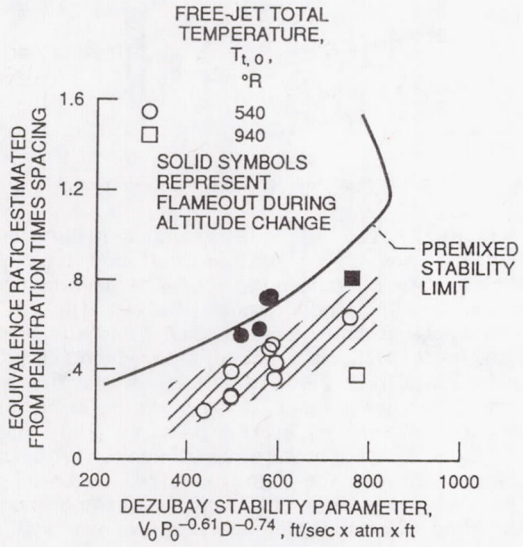

Fig. 13. Stability results.

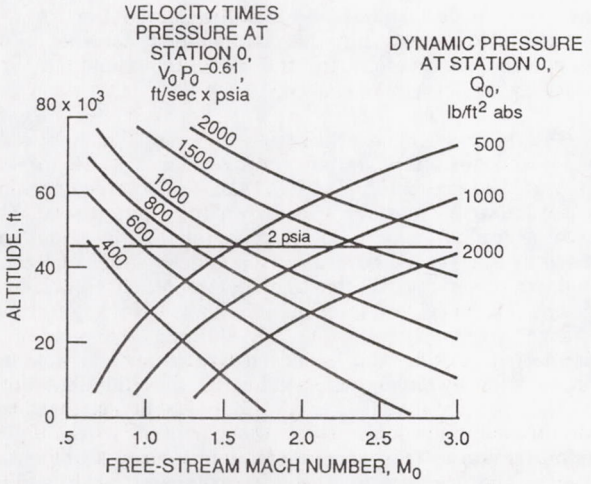

Fig. 14. Variation of DeZubay parameter with flight condition.

In subscale combustion tests the relative importance of chemical kinetics should be evaluated at least qualitatively. Ideally, the combustion process would be mixing limited and similar results would be obtained at larger scale as long as the appropriate similarity parameters were matched. In order to gain some insight into the effect of finite reaction rates on the plume at the present conditions and scale, two calibrated infrared images of the spraybar plume are compared in Fig. 15. The Reynolds and Mach numbers are the same for each; however, the free-stream pressure and temperature are different. In Fig. 15(a) the free-stream pressure and temperature are both roughly twice those in Fig. 15(b) at comparable equivalence ratio and jet penetration. In order to see the potential this creates for a change in the reaction rate, the reaction time correlation of Pergament[32] was extrapolated to the present conditions; it predicts a reaction length for Fig. 15(b) that is a factor of 3 greater than that of Fig. 15(a). If the flow were premixed and completely reaction rate limited, this would result in a substantial change in the plume temperature contours. On the other hand, if the flow were completely mixing limited, the plumes should appear similar. Because a difference in the plume characteristics is apparent, it may be concluded that chemical reaction rates do have an effect on the plume characteristics at this Reynolds number. This undesirable result is not of great consequence for the flame stability results, since the correlating parameters contain appropriate length scales and the spraybars were probably not too far from full scale anyway. The issue will be with subscale tests of the entire external burning process, where reaction rates and model scale may have a significant effect on the resultant pressure distributions. Fortunately, it would seem that these problems, while making data interpretation difficult, will lead to conservative results. If external burning is successful in small scale, confidence in full-scale success is increased greatly.

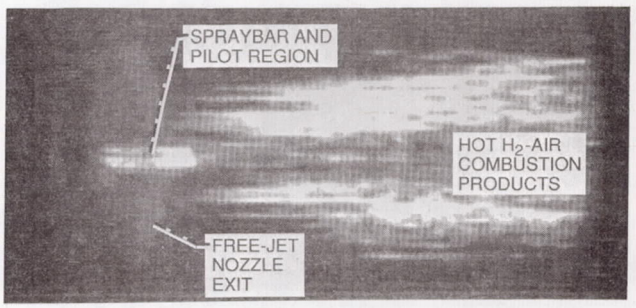

(a) Free-stream static pressure, P_0, 12 psia; free-stream total temperature, $T_{t,0}$, 960 °R; equivalence ratio, ϕ, 0.48; jet penetration height, Y_p, 0.72 in.

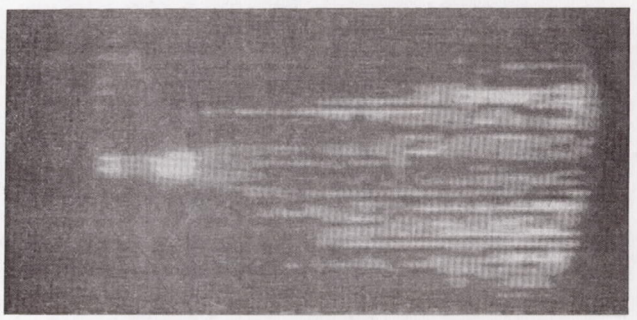

(b) Free-stream static pressure, P_0, 6 psia; free-stream total temperature, $T_{t,0}$, 540 °R; equivalence ratio, ϕ, 0.51; jet penetration height, Y_p, 1.0 in.

Fig. 15. Infrared images of plume at Reynolds number of 4.8 million per foot. Black areas are <1000 °R; white areas are 3400 °R.

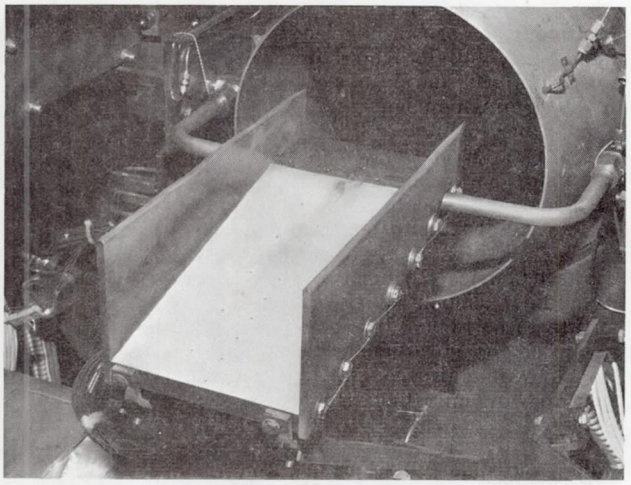

Fig. 16. Expansion ramp model with upper sidewalls mounted in free jet.

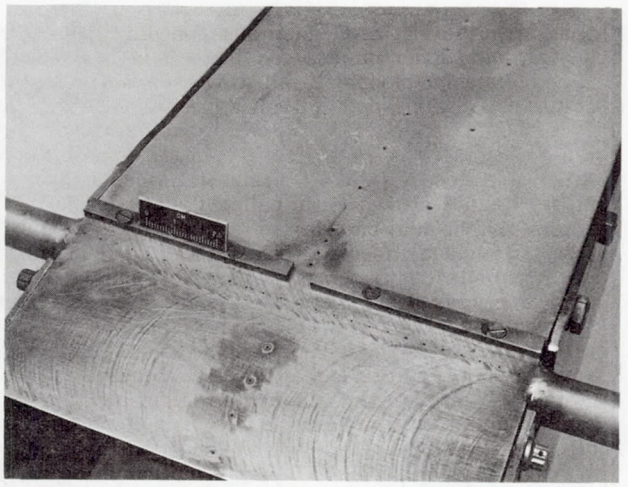

Fig. 17. Expansion ramp fuel injection and flameholding region.

Expansion Ramp Tests

Apparatus and procedure. - The expansion ramp tests were intended to demonstrate drag reduction on a simple expansion ramp geometry while providing calibration and verification information for analysis methods. No changes were made to the facility, and the expansion ramp models were mounted in the free jet in much the same way as the spraybar models. The basic configuration, shown in Fig. 16, consisted of a 3- by 6-in. flat plate with a sharp leading edge, followed by an 11.2- by 6-in. expansion ramp. Two similar expansion ramps were tested, the only difference between the two being the spacing and diameter of the fuel injection orifices. The models were constructed of a single piece of 3/4-in.-thick stainless steel with a zirconium-oxide coating sprayed on the expansion surface. Upper sidewalls extending 2 in. above the leading edge are shown, but the models were tested primarily with lower sidewalls that were flush with the upper surface and extended 2 in. below the model at the trailing edge. The lower sidewalls were intended to keep high-pressure air generated by compression beneath the model from spilling around and affecting pressure distributions on the top surface. Fuel was injected normal to the free-jet axis through a row of choked orifices in a plane 1/2 in. upstream of the expansion corner. A flameholder was used to ensure combustion at the desired location and consisted of a 1/4-in.-wide by 1/8-in.-high strip of stainless steel spanning the entire 6-in. width of the model with a 1/4-in. gap in the center to allow for thermal expansion. The trailing edge of the flameholder was coincident with the expansion corner. Details of the fuel injection and flameholder arrangement are given in Fig. 17. The configuration pictured had twenty-six 0.025-in.-diameter orifices equally spaced across the 6-in. width to provide a range of equivalence ratios from 0.4 to 1.2. The other had eight 0.044-in. injectors designed for somewhat lower equivalence ratios from 0.2 to 0.7.

Figure 18 depicts the location of instrumentation with respect to the expansion ramp models. The only change from the spraybar tests is the addition of static pressure and temperature instrumentation on the upper surface of the models. A single, centerline row of 18 static pressure taps and an off-centerline row of 5 thermocouples were used.

The expansion ramp tests were all run at the ambient free-jet total temperature of 540 °R. Because the gas generator was not available during these tests, only ambient-temperature hydrogen fuel was used.

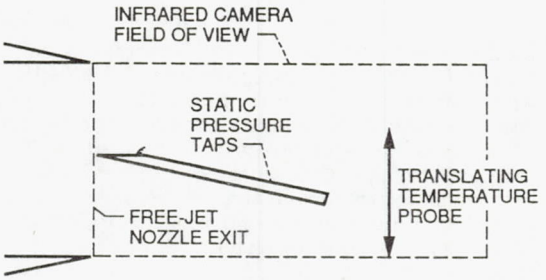

Fig. 18. Expansion ramp test instrumentation.

Results. - The higher-equivalence-ratio model (26 injectors) was tested first without any type of flameholder. Model ignition could only be accomplished at a subsonic free-jet Mach number of about 0.6. As the free-jet supply pressure was increased and the design Mach number of 1.26 was reached, color video and infrared images indicated that the leading edge of the flame was anchored at a point about halfway down the ramp surface probably at the boundary layer separation point, having little effect on the pressure distribution. With the flameholder installed the flame remained anchored near the flameholder trailing edge, but supersonic model ignition using the translating spark ignitor was still not possible. The inability to ignite the supersonic stream should not be taken as a general result, however, since the arc location is a critical parameter that was not varied. The low-equivalence-ratio model was ignited in subsonic flow as well but would not sustain combustion in supersonic flow even with the flameholder installed. For this reason, only results for the high-equivalence-ratio, 26-orifice model are presented.

Model centerline static pressure distributions with the lower sidewalls installed are shown in Fig. 19 for a range of fuel pressures. Fuel-off and fuel-on (not burning) pressure distributions are also shown for comparison. The pressure gradient on the forward portion of the model was caused by a detached bow shock on the leading edge that could not be made thin enough for the Mach 1.26 free stream. The effect of the flameholder is also apparent as a large overpressure. The no-burning pressure distributions exhibit the expected overexpansion at the 3-in. station, which corresponded to the flameholder trailing edge and model "knee." Boundary layer separation and three-dimensional relief then caused a rapid recompression to free-stream static pressure. Combustion affected the pressure all the way upstream to the leading edge and eliminated much of the large overexpansion at

the model knee, creating a region of relatively constant pressure over the ramp surface. The combustion pressure remained below the free-stream value, however, and showed little variation with fuel pressure in contrast to the control-volume prediction, even though both the jet penetration and the estimated equivalence ratio were increasing markedly.

The estimated jet penetration was based on an X/d* of 30 in Eq. (6). This resulted in a good correlation between the measured maximum plume temperature and the estimated equivalence ratio for all altitudes and fuel pressures. The maximum plume temperatures were, however, somewhat lower than the theoretical equilibrium temperature at the correlated equivalence ratio. In order to provide a better (or at least more conservative) model of the station 2 conditions, a combustion efficiency was added to the control-volume procedure so that for any altitude and fuel pressure the calculated temperature at station 2 approximately matched the measured maximum plume temperature. This is the basis for the "control-volume predictions" in Figs. 19 to 23.

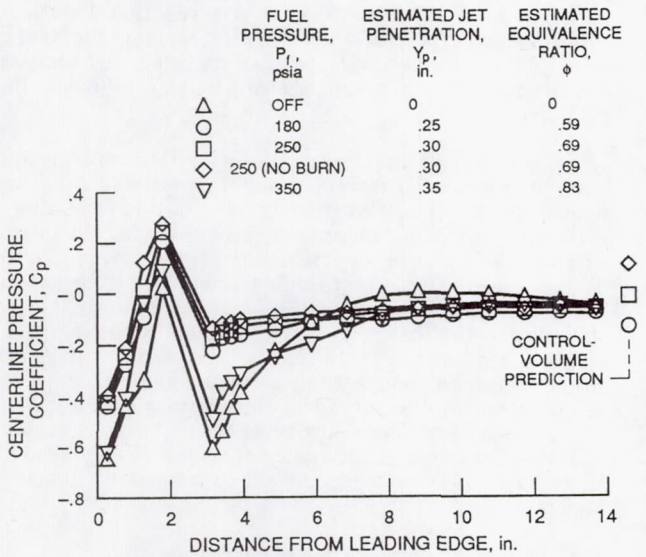

Fig. 19. Effect of increasing fuel pressure on ramp surface static pressure distributions. Free-stream static pressure, P_0, 8 psia.

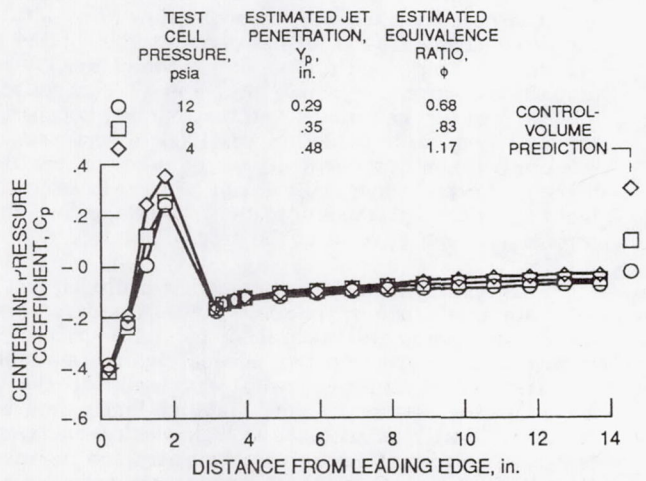

Fig. 20. Effect of increasing altitude on ramp surface static pressure distributions. Fuel pressure, P_f, 350 psia.

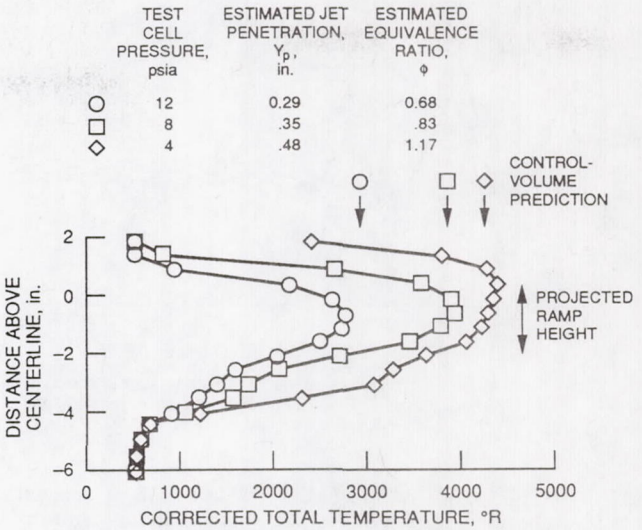

Fig. 21. Effect of increasing altitude on plume total temperature profiles. Fuel pressure, P_f, 350 psia.

(a) Free-stream static pressure, P_0, 12 psia (5500 ft).

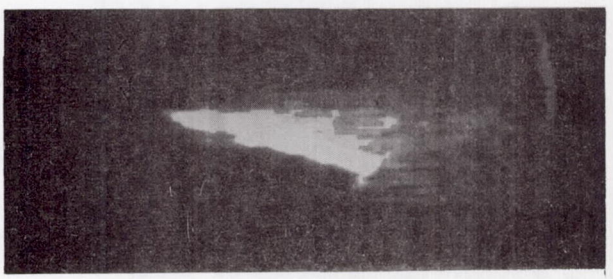

(b) Free-stream static pressure, P_0, 8 psia (16 000 ft).

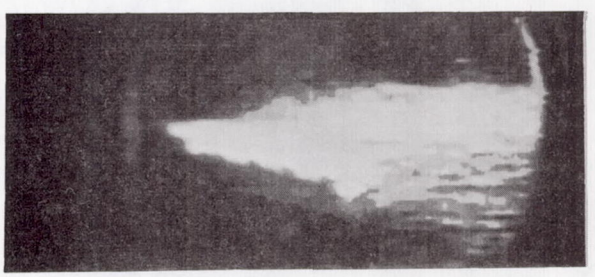

(c) Free-stream static pressure, P_0, 4 psia (32 000 ft).

Fig. 22. Infrared images of plume at various altitudes. Fuel pressure, P_f, 350 psia.

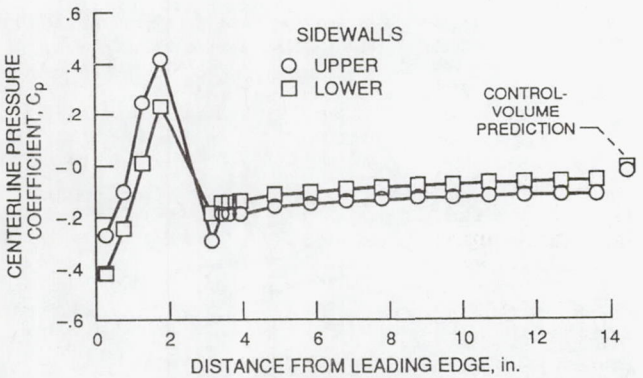

Fig. 23. Effect of sidewalls on ramp pressure distribution. Fuel pressure, P_f = 250 psia; estimated jet penetration, Y_p, 0.30; estimated equivalence ratio, ϕ, 0.70.

The effect of increasing the altitude at a constant fuel pressure, shown in Fig. 20, was much the same as the effect of increasing the fuel pressure; both equivalence ratio and jet penetration increased without affecting the combustion pressure. Very little variation in combustion pressure was noted over the entire range of altitudes and fuel pressures despite a factor-of-2 variation in both the jet penetration and the estimated equivalence ratio.

Plume total temperature profiles corresponding to the three conditions of the previous figure are shown in Fig. 21. The plume temperature and size both increased with altitude, as jet penetration and equivalence ratio increased. Obviously, the control-volume predictions show good agreement with the maximum plume temperatures, since the procedure was calibrated by using these data. The fact that measured plume temperatures did reach the theoretical maximum for hydrogen and air is encouraging. Calibrated infrared images given in Fig. 22 for the conditions of the previous figure show large changes in both the temperature and extent of the plume, with the plume apparently "filling" the base region.

The effect of upper sidewalls on the model centerline static pressure distribution is shown in Fig. 23. These sidewalls (pictured in Fig. 16) extended 2 in. above the model at the leading edge and had the expected effect of limiting three-dimensional relief. Since pressure was below the free-stream static without sidewalls, the effect of the sidewalls was to slightly lower the ramp pressure. A two-dimensional expansion assumption was used in the control-volume analysis to model this effect.

Lower than predicted ramp pressures in all cases could be due to a number of factors including the inherent assumption in the control-volume analysis that the control volume acts as a solid body to the free stream. The effects of nonuniform inflow and outflow and flameholder drag were neglected and could lead to discrepancies. Another source of uncertainty lay with the experimental apparatus itself as discussed in the next section.

Factors Influencing Test Results

The results obtained to date with the expansion ramp model are somewhat curious in nature given the vigorous combustion demonstrated and the lack of agreement with the control-volume analysis. Figure 24 depicts phenomena, currently being investigated in follow-on tests, that may possibly have influenced the static pressure distribution on the expansion ramp. One of the unique features of the external burning flowfield is the constant-pressure, constant-velocity plume, which resulted in a subsonic condition downstream of the model.

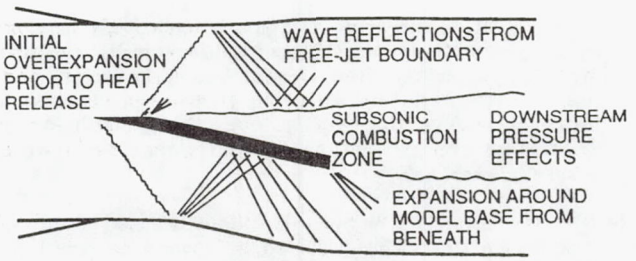

Fig. 24. Factors influencing test results.

Further, only a small velocity gradient existed between the subsonic plume and the supersonic free stream so that the subsonic condition could persist for large distances downstream of the model. Since upstream communication was possible within this subsonic core, reflected disturbances, the facility exhaust collector, expansion around the model base from beneath, or anything else causing a pressure perturbation downstream of the model could influence the ramp static pressure.

The slight overexpansion still present at the model knee with external burning may be due to a delay in the onset of heat release. Mixing and reaction kinetics probably both played a role here. Moving the fuel injection and flameholding farther upstream and increasing the free-stream temperature will help to alleviate this problem.

Finally, the necessity of using a flameholder could lead to unexpected results, since flameholder drag was neglected in the control-volume analysis. Testing different size flameholders may give some insight into this effect; however, the use of a flameholder gives rise to a scaling issue. The 1/8-in.-high flameholder used extended a significant distance into the fueled stream. If this were scaled geometrically to give similar aerodynamic characteristics to a large test article, a prohibitive drag would result. Although from a flameholding standpoint it is not necessary to scale the flameholder geometrically, the mechanics of flame spreading from the pilot region to the outer reaches of the fueled stream will only be similar if the ratio of flameholder height to jet penetration is held constant.

Summary and Conclusions

External burning, used in conjunction with a variable cowl flap to prevent exhaust flow overexpansion, is a promising transonic drag reduction concept. Results of a simple control-volume analysis indicate that transonic drag can be eliminated with hydrogen flow rates of 0.1 to 0.2 lb/sec per square foot of base area at 1000-lb/ft^2 abs dynamic pressure, with fuel flows being roughly proportional to the dynamic pressure. The specific impulse performance of the external burning scheme in terms of drag force reduction was 1000 to 3000 sec and was proportional to the severity of the drag force without burning. Normal sonic orifices can be used to inject the fuel the required distance into the free stream, which is approximately 10 percent of the base height.

Experimental results indicate that hydrogen and air will burn at altitude in transonic flow. A flame stability correlation parameter published for a premixed hydrogen-air stream worked adequately if a suitable definition of equivalence ratio was used for the non-premixed stream. Flame stability limits may be encountered at high altitude, at high Mach number, or both. The effect of finite rate chemistry and the use of flameholders make scaling of small-scale test results difficult. The external burning process was used to

increase pressures on a small expansion ramp at Mach 1.26 to altitudes of 32 000 ft, but measured performance was not as high as predicted by the control-volume analysis. Ramp pressure showed little variation with fuel pressure and altitude despite large changes in the temperature and size of the plume; plume temperatures equal to the theoretical maximum for hydrogen and air were recorded just downstream of the expansion ramp. A number of reasons for these discrepancies, including anomalous facility effects, were discussed. The nearly constant-velocity nature of the external burning process presents a unique challenge to the experimentalist in providing a disturbance-free test medium. Some form of atmospheric or flight test may be required to completely resolve the magnitude of the external burning benefit. Also, finite chemical reaction times at these conditions and the use of an unscaled flameholder may necessitate testing at large scale, depending on the degree of confidence desired in the full-scale result.

References

1. Keyworth, G.A., II, "National Aeronautical R&D Goals," Aeronautical Policy Review Board, Executive Office of the President, Office of Science and Technology Policy, Washington, DC, 20500, March 1985.

2. Murthy, S.N.B., ed., et al., Aerodynamics of Base Combustion, MIT Press, Cambridge, 1976, pp. 143-210.

3. Dorsch, R.G., Serafini, J.S. and Fletcher, E.A., "Exploratory Investigation of Aerodynamic Effects of External Combustion of Aluminum Borohydride in Airstream Adjacent to Flat Plate in Mach 2.46 Tunnel," NACA RM E57E16, 1957.

4. Dorsch, R.G., Serafini, J.S. and Fletcher, E.A., "Experimental Investigation of Aerodynamic Effects of External Combustion in Airstream Below Two-Dimensional Supersonic Wing at Mach 2.5 and 3.0," NASA memo 1-11-59E, 1959.

5. Serafini, J.S., Dorsch, R.G. and Fletcher, E.A., "Exploratory Investigation of Static- and Base-Pressure Increases Resulting From Combustion of Aluminum Borohydride Adjacent to Body of Revolution in Supersonic Wind Tunnel," NACA RM E57E15, 1957.

6. Schadow, K.C., "Experimental Investigation of Combined External Burning/Base Burning," AIAA, SAE, ASME 17th Joint Propulsion Conference, Hardford, CT, 1980.

7. Hubbartt, J.E. and Strahle, W.C., "External/Base Burning for Base Drag Reduction at Mach 3," AIAA Journal, Vol. 19, Nov. 1981, pp. 1502-1504.

8. Caswell, G.J., "Base Drag Reduction by External Burning in the Inviscid Stream," M.S. Thesis, Naval Postgraduate School, Monterey, CA, Sept. 1973.

9. Reding, J.P. and Jecmen, D.M., "Effects of External Burning on Spike-Induced Separated Flow," AIAA Paper 82-1360, Aug. 1982.

10. Billig, F.S., "External Burning in Supersonic Streams," Johns Hopkins University Applied Physics Laboratory, TG-912, May 1967.

11. Dugger, G.L. and Monchick, L., "External Burning Ramjets, Preliminary Feasibility Study," Johns Hopkins University Applied Physics Laboratory, TG-892, Mar. 1967.

12. Strahle, W.C., "Some Outer Limits in the Theory of Transonic Flow With External Burning," Combustion Science and Technology, Vol. 1, Apr. 1970, pp. 357-363.

13. Pinkel, I.I., Serafini, J.S. and Gregg, J.L., "Pressure Distribution and Aerodynamic Coefficients Associated With Heat Addition to Supersonic Air Stream Adjacent to Two-Dimensional Supersonic Wing," NACA RM E51K26, 1952.

14. Schetz, J.A., Billig, F.S. and Favin, S., "Approximate Analysis of Base Drag Reduction by Base and/or External Burning for Axisymmetric, Supersonic Bodies," AIAA Paper 80-1258, June 1980.

15. Mehta, G.K. and Strahle, W.C., "Analysis of Axially Symmetric External Burning Propulsion for Bluff-Base Bodies," AIAA Paper 78-26, Jan. 1978.

16. Broadbent, E.G., "Flows With Heat Addition and Associated Pressure Fields," Fluid Dynamic Transactions, Vol. 6, Pt. 1, 1972, pp. 80-113.

17. Smithey, W. and Fuhs, A.E., "Base Pressure Calculations With External Burning," in Aerodynamics of Base Combustion, MIT Press, Cambridge, 1976, pp. 407-424.

18. Marino, A., "Theoretical Performance With External Burning on Surface," General Applied Science Labs, Inc., Westbury, New York, GASL TR-506, Feb. 1965.

19. Oswatitsch, K., "Thrust and Drag With Heat Addition to a Supersonic Flow," R.A.E. Library Translation No. 1161, January 1967 (Summary report presented to the 3rd Euromech Symposium, Aachen, Feb. 1966).

20. Harvey, D.W. and Davis, J.C., "External Burning Propulsion Analysis," AIAA Paper 81-1477, July 1981.

21. Adamson, T.C., Jr., and Nicholls, J.A., "On the Structure of Jets From Highly Underexpanded Nozzles Into Still Air," Journal of the Aero/Space Sciences, Jan. 1959, pp. 16-24.

22. Zukoski, E.E. and Spaid, F.W., "Secondary Injection of Gases Into a Supersonic Flow," AIAA Journal, Vol. 2, Oct. 1964, pp. 1689-1696.

23. Crist, S., Sherman, P.M. and Glass, D.R., "Study of the Highly Underexpanded Sonic Jet," AIAA Journal, Vol. 4, Jan. 1966, pp. 68-71.

24. Schetz, J.A. and Billig, F.S., "Penetration of Gaseous Jets Injected Into a Supersonic Stream," J. Spacecraft, Vol. 3, Nov. 1966, pp. 1658-1665.

25. Schetz, J.A., Hawkins, P.F. and Lehman, H., "Structure of Highly Underexpanded Transverse Jets in a Supersonic Stream," AIAA Journal, Vol. 5, May 1967, pp. 882-884.

26. Chrans, L.J. and Collins, D.J., "Stagnation Temperature and Molecular Weight Effects in Jet Interaction," AIAA Journal, Vol. 8, Feb. 1970, pp. 287-293.

27. Hersch, M., Povinelli, L.A. and Povinelli, F.P., "Optical Study of Sonic and Supersonic Jet Penetration From a Flat Plate Into a Mach 2 Airstream," NASA TN D-5717, Mar. 1970.

28. Povinelli, F.P. and Povinelli, L.A., "Correlation of Secondary Sonic and Supersonic Gaseous Jet Penetration Into Supersonic Crossflows," NASA TN D-6370, June 1971.

29. Billig, F.S., Orth, R.C. and Lasky, M., "A Unified Analysis of Gaseous Jet Penetration," AIAA Journal, Vol. 9, June 1971, pp. 1048-1058.

30. Orth, R.C., Schetz, J.A. and Billig, F.S., "The Interaction and Penetration of Gaseous Jets in Supersonic Flow," NASA CR-1386, 1969.

31. DeZubay, E.A., "A Study of Flame Stability Based on Reaction Rate Theory," ASME Paper 54-SA-27, May 1954.

32. Huber, P.W., Schexnayder, C.J. and McClinton, C.R., "Criterion for Self-Ignition of Supersonic Hydrogen-Air Mixtures," NASA TP-1457, 1979.

NASA
National Aeronautics and Space Administration

Report Documentation Page

1. Report No.	2. Government Accession No.	3. Recipient's Catalog No.
NASA TM-103107 AIAA-90-1935		

4. Title and Subtitle

On the Use of External Burning to Reduce Aerospace Vehicle Transonic Drag

5. Report Date

6. Performing Organization Code

7. Author(s)

Charles J. Trefny

8. Performing Organization Report No.

E-5431

10. Work Unit No.

763-01-21

9. Performing Organization Name and Address

National Aeronautics and Space Administration
Lewis Research Center
Cleveland, Ohio 44135-3191

11. Contract or Grant No.

13. Type of Report and Period Covered

Technical Memorandum

12. Sponsoring Agency Name and Address

National Aeronautics and Space Administration
Washington, D.C. 20546-0001

14. Sponsoring Agency Code

15. Supplementary Notes

Prepared for the 26th Joint Propulsion Conference cosponsored by the AIAA, ASME, SAE, and ASEE, Orlando, Florida, July 16-18, 1990.

16. Abstract

The external combustion of hydrogen to reduce the transonic drag of aerospace vehicles is currently being investigated. A preliminary analysis based on a constant-pressure control volume is discussed. Results indicate that the specific impulse of the external burning process rivals that of a turbojet and depends on the severity of the initial base drag as well as on the flight Mach number and the equivalence ratio. A test program was conducted to investigate hydrogen-air flame stability at the conditions of interest and to demonstrate drag reduction on a simple expansion ramp. Initial test results are presented and compared with the control-volume analysis. The expansion ramp surface pressure coefficient showed little variation with fuel pressure and altitude—in disagreement with the analysis. Flame stability results were encouraging and indicate that stable combustion is possible over an adequate range of conditions. Facility interference and chemical kinetics phenomena that make interpretation of subscale ground test data difficult are discussed.

17. Key Words (Suggested by Author(s))	18. Distribution Statement
External burning Transonic drag reduction	Unclassified – Unlimited Subject Category 07

19. Security Classif. (of this report)	20. Security Classif. (of this page)	21. No. of pages	22. Price*
Unclassified	Unclassified	16	A03

*For sale by the National Technical Information Service, Springfield, Virginia 22161